AFATL-TR-72-181

FLIGHT DYNAMICS AND DISPERSION CHARACTERISTICS OF S-CURVE AND ROLL-THROUGH-ZERO BOMBLETS

ALPHA RESEARCH, INC.

TECHNICAL REPORT AFATL-TR-72-181

SEPTEMBER 1972

Approved for public release; distribution unlimited.

AIR FORCE ARMAMENT LABORATORY
AIR FORCE SYSTEMS COMMAND • UNITED STATES AIR FORCE
EGLIN AIR FORCE BASE, FLORIDA

Security Classification

DOCUMENT CONTROL DATA - R & D

(Security classification of title, body of abstract and indexing annotation must be entered when the overall report is classified)

1 ORIGINATING ACTIVITY (Corporate author) Alpha Research, Inc. Santa Barbara, Calif.	2a. REPORT SECURITY CLASSIFICATION UNCLASSIFIED 2b. GROUP

3 REPORT TITLE

FLIGHT DYNAMICS AND DISPERSION CHARACTERISTICS OF S-CURVE AND ROLL-THROUGH-ZERO BOMBLETS

4 DESCRIPTIVE NOTES (Type of report and inclusive dates)

Final Report - June 1970 to September 1972

5 AUTHOR(S) (First name, middle initial, last name)

James E. Brunk

6 REPORT DATE September 1972	7a. TOTAL NO. OF PAGES 42	7b. NO. OF REFS 10
8a. CONTRACT OR GRANT NO F08635-70-C-0012 F08635-71-C-0089 b. PROJECT NO 2547 c. Task No. 01 d. Work Unit Code No. 020	9a. ORIGINATOR'S REPORT NUMBER(S) 9b. OTHER REPORT NO(S) (Any other numbers that may be assigned this report) AFATL-TR-72-181	

10 DISTRIBUTION STATEMENT

Approved for public release; distribution unlimited.

11 SUPPLEMENTARY NOTES Available in DDC	12. SPONSORING MILITARY ACTIVITY Air Force Armament Laboratory Air Force Systems Command Eglin Air Force Base, Florida 32542

13 ABSTRACT

Two new ballistic-type self-dispersing bomblets which utilize passive control of the radial orientation of the trimmed lift force are described and the motion of these bomblets as determined by simplified theory and by exact six-degree-of-freedom simulation is discussed. Some of the unique aerodynamic characteristics of these bomblets as determined from wind tunnel tests are also described. Impact pattern predictions, using the Monte Carlo method, show that properly designed S-Curve and roll-through-zero bomblets can achieve large uniform patterns for low-altitude high-speed delivery conditions; however, configurational asymmetries, if not suitably restricted, can significantly modify the bomblet performance.

DD FORM 1 NOV 65 1473

1a

UNCLASSIFIED
Security Classification

14 KEY WORDS	LINK A		LINK B		LINK C	
	ROLE	WT	ROLE	WT	ROLE	WT
S-Curve Bomblet						
Roll-Through-Zero Bomblet						
Ballistic-Type Self-Dispersing Bomblets						
Six-Degrees-of-Freedom Simulation						
Monte Carlo Dispersion						
Monte Carlo Impact-Dispersion Patterns						
Cylindrical Afterbody						
Boattail Afterbody						

1b

Flight Dynamics And Dispersion Characteristics Of S-Curve And Roll-Through-Zero Bomblets

James E. Brunk

10

FOREWORD

This report documents work performed during the period June 1970 to September 1972 by Alpha Research, Inc., Santa Barbara, California, under contracts F08635-70-C-0012 and F08635-71-C-0089 with the Air Force Armament Laboratory, Eglin Air Force Base, Florida 32542. Second Lieutenant Paul C. Mayer (DLDL) monitored the program for the Armament Laboratory.

The report has been reviewed and is approved.

DALE M. DAVIS
Chief, Guns and Rockets Division

ABSTRACT

Two new ballistic-type self-dispersing bomblets which utilize passive control of the radial orientation of the trimmed lift force are described and the motion of these bomblets as determined by simplified theory and by exact six-degrees-of-freedom simulation is discussed. Some of the unique aerodynamic characteristics of these bomblets as determined from wind tunnel tests are also described. Impact pattern predictions, using the Monte Carlo method, show that properly designed S-Curve and roll-through-zero bomblets can achieve large uniform patterns for low-altitude high-speed delivery conditions; however, configurational asymmetries, if not suitably restricted, can significantly modify the bomblet performance.

(The reverse of this page is blank)

TABLE OF CONTENTS

LIST OF FIGURES

LIST OF FIGURES (CONCLUDED)

LIST OF TABLES

LIST OF ABBREVIATIONS AND SYMBOLS

C_ℓ	Roll torque coefficient
C_{ℓ_o}	Roll torque coefficient at $p = 0$
C_{ℓ_δ}	Roll torque coefficient due to surface deflection
C_M	Pitching moment coefficient
C_{M_p}	Magnus moment coefficient; $\frac{pd}{2V}$
C_{S_M}	Side moment coefficient
C_N	Normal force coefficient
C_{N_T}	Trimmed normal force coefficient
C_{n_r}	Circular yaw damping derivative; $\frac{rd}{2V}$
d	Aerodynamic reference length, ft (body diameter)
g	Acceleration due to gravity, ft/sec^2
h	Altitude, ft
I_x	Axial moment of inertia, $slug\text{-}ft^2$
I_x'	$I_x/\rho\, Sd^3$, nondimensional inertia
I	Transverse moment of inertia, $slug\text{-}ft^2$
m	Mass, slugs
n	Number of fins
p	Roll rate, rad/sec
q	Pitch rate, rad/sec
q*	Pitch rate, angle of attack plane, rad/sec
r	Yaw rate, rad/sec
S	Aerodynamic reference area, $\pi d^2/4$, ft^2
t	Time, seconds
V	Velocity ft/sec

V_E	Velocity at dispenser function, ft/sec
V_R	Radial velocity at cluster break-out, ft/sec
x, y, z	Body axes, x is axis of asymmetry.
y_e', z_e'	Earth-fixed axes perpendicular to line of flight
$\vec{\alpha}$	Total angle of attack
α_T	Trim angle of attack
γ	Flight path angle with respect to horizontal
δ	Fin deflection
ρ	Air density
ϕ	Roll angle of body axes
$\tilde{\phi}$, $\overline{\Phi}$	Angle of attack plane orientation from vertical and horizontal planes, respectively (see Figure 4)
Φ	Aerodynamic roll angle (see Figure 4)

(The reverse of this page is blank)

SECTION I

INTRODUCTION

The increasing utilization of cluster-type weapons for tactical warfare has led to the need to consider various bomblet dispersion techniques. During the past several years two new self-dispersing bomblet concepts which utilize the lift force resulting from body incidence as a means of obtaining dispersion have been investigated. Each employs a novel means of passively restricting the rotation of the lift vector about the flight path as a means of greatly increasing the dispersion potential in the presence of configurational asymmetries.

The S-Curve bomblet is comprised of an axially symmetric body-fin configuration which is designed to provide an unstable restoring moment at small angle of attack and a stable pitching moment slope at a large trim angle of attack. The S-Curve name is derived from the shape of the nonlinear pitching moment curve. The salient feature of the S-Curve-type bomblet is that the trim incidence is independent of body-roll attitude such that the direction of the lift force vector with respect to a vertical plane is either fixed or slowly changing, even though the bomblet has an accidental spin. The use of this idea for bomblet dispersion was first described by Marchant and Pope.[1]

The roll-through-zero bomblet is comprised of a lifting-body configuration equipped with a roll producing device which will cause the bomblet to roll in a direction opposite to its initial direction of roll. The dispersion of this type bomblet depends upon the temporary and limited change in the orientation of the lift vector as the bomblet passes through zero roll. The fact that large dispersion can result from a roll-through-zero motion has been noted earlier with respect to the development of re-entry vehicles.[2]

This report describes the analytical dispersion predictions for several candidate S-Curve and roll-through-zero bomblet configurations.

SECTION II

FLIGHT DYNAMICS

S-Curve Bomblet

Aerodynamic Characteristics. Two considerations dominate the design of the S-Curve bomblet: first, the attainment of a proper nonlinear restoring moment characteristic throughout the operating Mach number range; second, restriction of roll dependent aerodynamic forces and moments, particularly the side moment, which causes undesirable coning motion. The latter is accomplished by increasing the axial symmetry (e.g., number of fins) and by limiting the trim angle of attack. The S-Curve moment characteristics are obtained most effectually by a combination of nose rounding, boattailing, and utilization of very low aspect-ratio fins or sub-caliber stabilizers.

Figure 1 illustrates two basic S-Curve bomblet designs which have been extensively investigated in the wind tunnel.[3-7] Both are four calibers in length; however, the first has a cylindrical afterbody while the second has a boattail afterbody. Figure 2 illustrates the pitching moment, normal force, and trim characteristics of the two basic S-Curve configurations. The two S-Curve bomblet configurations differ essentially in their transonic trim characteristics. At transonic Mach number the cylindrical afterbody bomblet exhibits large variations in trim angle, while for the bomblet with the boattail afterbody the trim angle is nearly invariant with Mach number.

The induced roll torque and side moment coefficients at Φ = 15 degrees (approximately maximum values), as well as the magnus moment coefficient, are plotted in Figure 3 as a function of angle of attack for the cylindrical afterbody configuration. Two different magnus moment curves are plotted; the original estimate is based on test results of an Australian Defence Scientific Service Weapons Research Establishment designed S-curve bomblet,[8] and is used for some flight dynamic calculations which will be described later. All of the moments are high nonlinear functions of angle of attack; however, for trim angles of attack between 8 and 16 degrees the moments, with the exception of the side moment, are small.

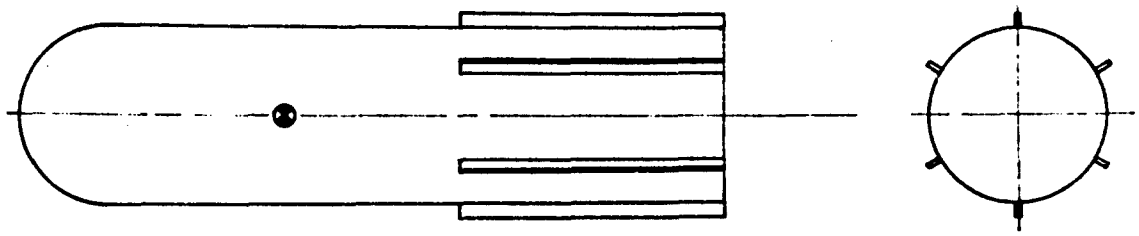

(a) S-Curve Bomblet: Cylindrical Afterbody

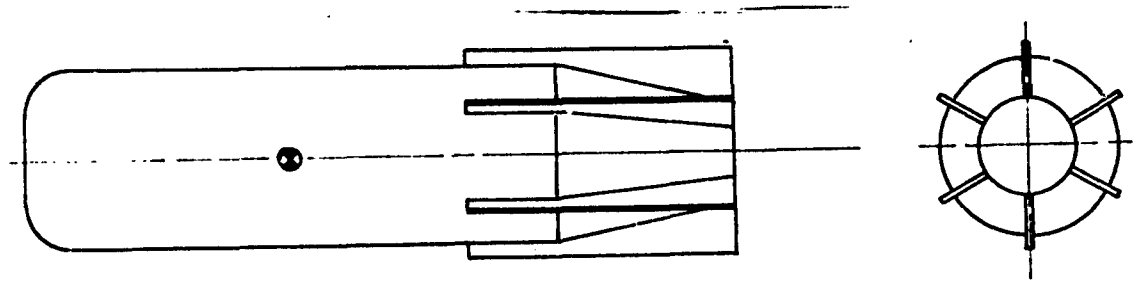

(b) S-Curve Bomblet: Boattail Afterbody

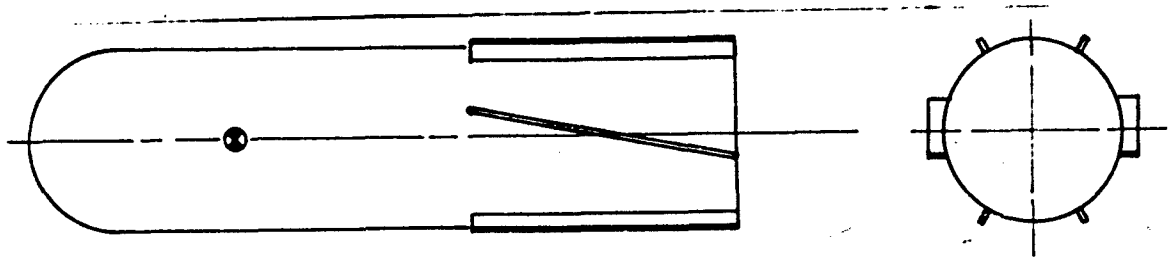

(c) Roll-Through-Zero Bomblet

Figure 1. Bomblet Configurations

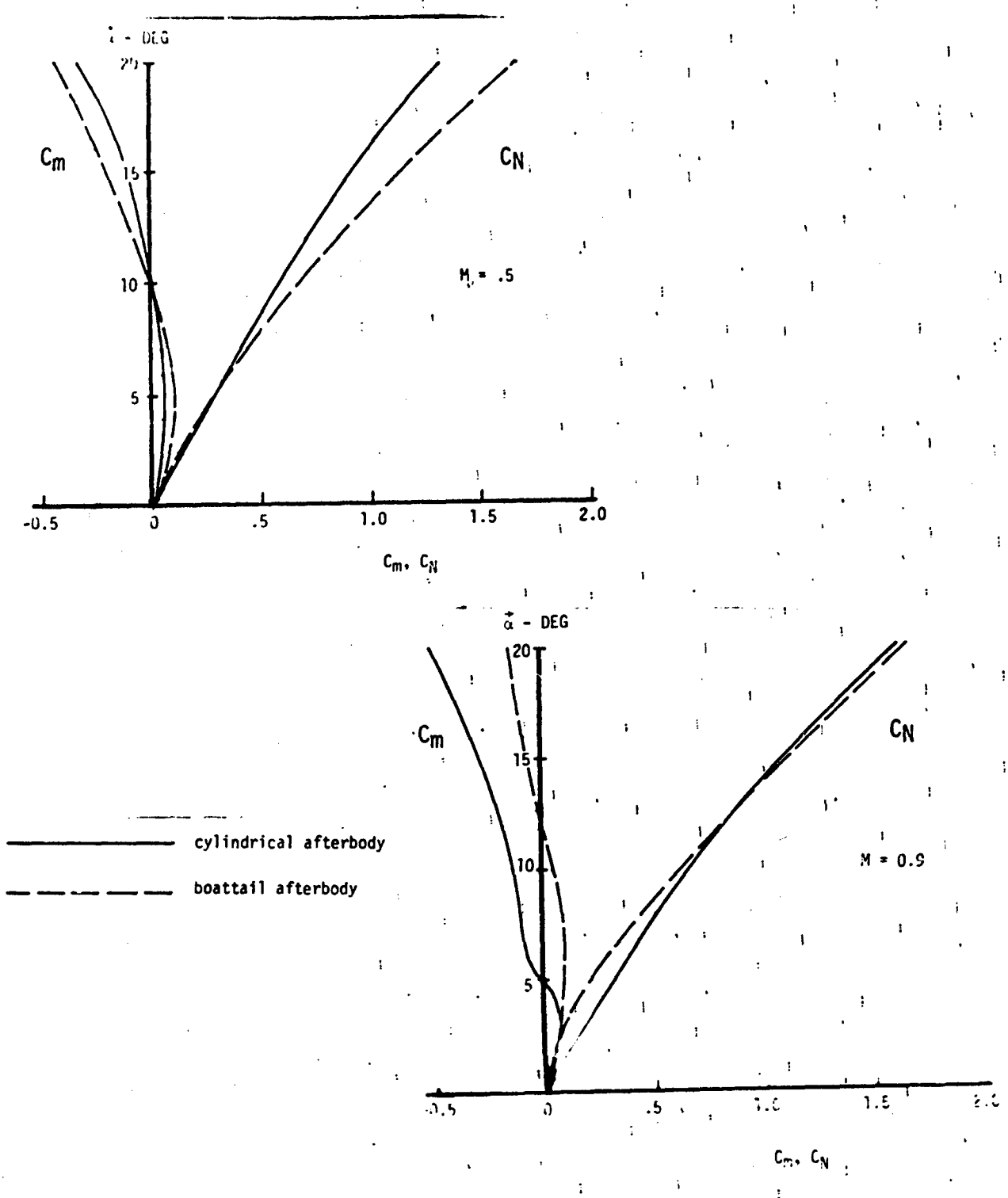

Figure 2. S-Curve Bomblet Normal Force, Pitching Moment and Trim Characteristics

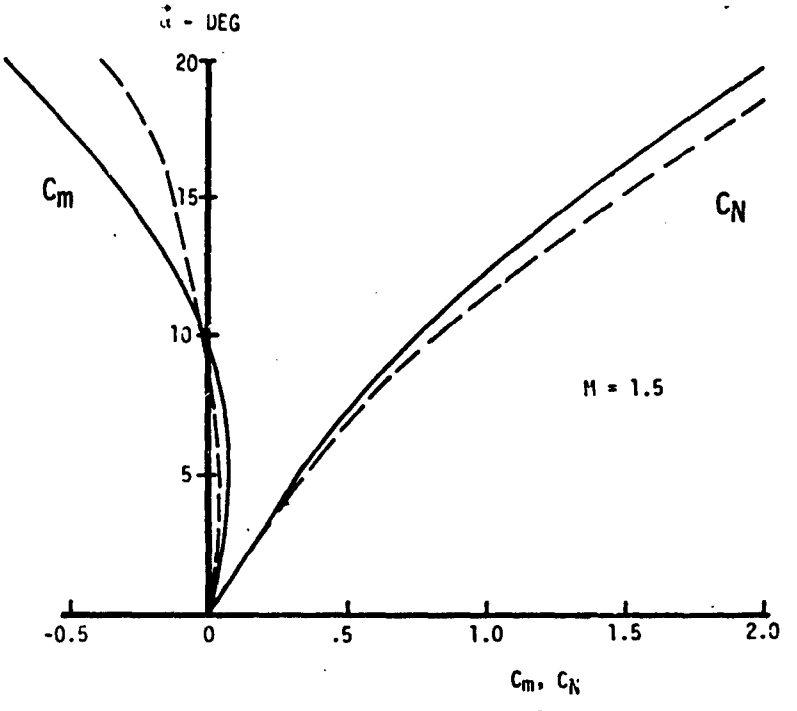

Figure 2. (Concluded)

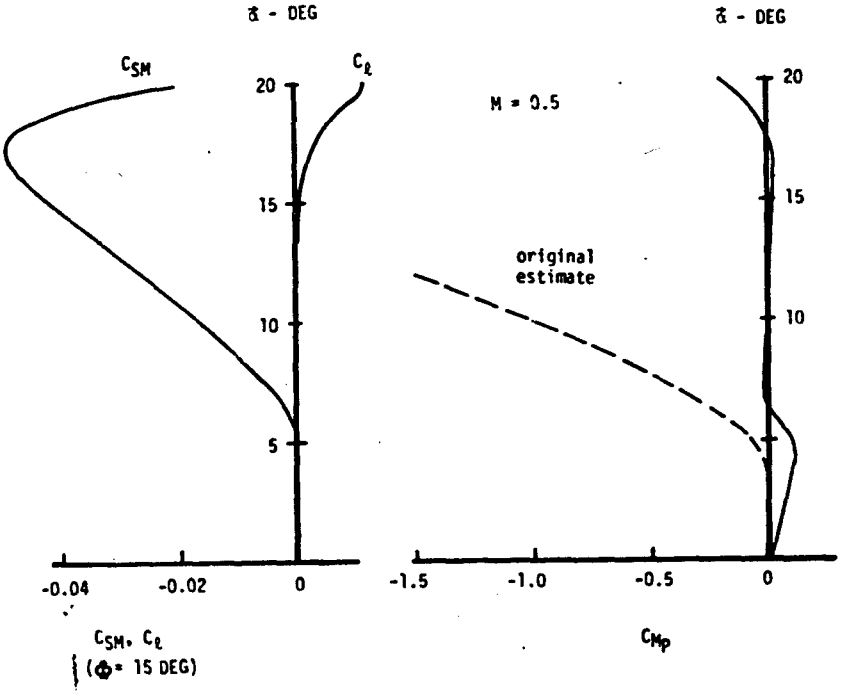

Figure 3. S-Curve Bomblet Magnus, Side Moment, and Roll Moment Characteristics.

Zero Coning Theory. The tendency for the angle of attack plane to remain stationary (i.e., for the coning to be zero) is the fundamental reason for the large dispersion of the S-Curve bomblet. The requirements for zero coning can be stated precisely by considering the differential equation for the variable, $\tilde{\phi}$, which is the orientation of the angle of attack plane with respect to a vertical reference plane.[9]

$$I \alpha_T \ddot{\tilde{\phi}} - \left[\frac{I g \alpha_T \sin\gamma}{V} - \frac{I C_N \rho S V}{2m} + \frac{C_{n_r} \rho S d^2 V \alpha_T}{4}\right] \dot{\tilde{\phi}}$$

$$+ \left[\frac{I_x p g \cos\gamma}{V}\right] \cos\tilde{\phi} - \left[\frac{C_{n_r} g \rho S d^2 \cos\gamma}{4}\right] \sin\tilde{\phi} = \tag{1}$$

$$\left[\frac{C_{M_p} \rho S d^2 V}{4} + \frac{I_x C_N \rho S V}{2m} - \frac{I_x g \alpha_T \sin}{V}\right] p$$

$$+ \frac{C_{SM} \rho V^2 S d}{2}$$

The existence of a steady-state solution for $\tilde{\phi}$ in Equation (1) is determined by setting $\dot{\tilde{\phi}} = \ddot{\tilde{\phi}} = 0$. This results in Equation (2),

$$p I_x \left[\frac{g \cos\gamma \cos\tilde{\phi}}{V} - \frac{C_N \rho S V}{2m} + \frac{g \alpha_T \sin\gamma}{}\right]$$

$$- \frac{C_{n_r} g \rho S d^2 \cos\gamma \sin\tilde{\phi}}{} - \frac{1}{4} C_{M_p} p \rho S d^2 V \tag{2}$$

$$- \frac{1}{2} C_{SM} \rho V^2 S d = 0$$

where the first term (in braces) is the gyroscopic moment due to rate of change of flight path curvature, the second term is the damping moment due to circular motion, and the third and fourth terms are the magnus and side moments, respectively. If the roll rate is very small, and the side moment negligible, then the roll rate dependent terms approach zero and the damping terms must also approach zero, implying that $\tilde{\phi}$ is near zero. For

the purpose of obtaining exact solutions for $\tilde{\phi}$, it is useful to consider the following alternative form of Equation (2).

$$A \cos \tilde{\phi} + B \sin \tilde{\phi} = C \tag{3}$$

where

$$A = p \left[\frac{I_x g \cos \gamma}{V} \right]$$

$$B = - \left[\frac{C_{n_r} g \rho S d^2 \cos \gamma}{4} \right]$$

$$C = p \left[\frac{C_{M_p} \rho S d^2 V}{4} + \frac{I_x C_N \rho S V}{2m} - \frac{I_x g \alpha_T \sin \gamma}{V} \right] + \frac{C_{SM} \rho S d V^2}{2}$$

Solutions to Equation (3) exist for

$$C^2 \leq A^2 + B^2$$

For flat trajectories ($\gamma \to 0$) the latter inequality can be expressed as

$$\left| \left[\frac{C_{M_p} \rho S d^2 V}{4} + \frac{I_x C_N \rho S V}{2m} \right] p + \frac{C_{SM} \rho S d V^2}{2} \right| \leq \left\{ \left[\frac{I_x g p}{V} \right]^2 + \left[\frac{C_{n_r} g \rho S d^2}{4} \right]^2 \right\}^{\frac{1}{2}} \tag{4}$$

Examination of (4) reveals that large values of p, C_{M_p}, or C_{SM} preclude the attainment of a solution for $\tilde{\phi}$, while large damping C_{n_r}, makes a solution more likely. However, if C_{SM} is small and can be neglected, there may be a range of $| p | < | pcr |$ for which solutions for $\tilde{\phi}$ exist. In such cases, we will define P_{CR} as the critical roll rate. At roll rates less than the critical rate, the coning rate is zero; at roll rates greater than the critical roll rate, the coning rate is finite.

Under those conditions where a solution for $\tilde{\phi}$ is possible, it is worthwhile to examine the nature of the solutions. First, consider the case where C_{SM} is negligible and only C_{M_p} is important. It is found from Equation (2) that the variation of $\tilde{\phi}$ with p for $|p| < |p_{CR}|$ is typically like the result plotted in Figure 4, which was computed using the original estimate for C_{M_p} in Figure 3.

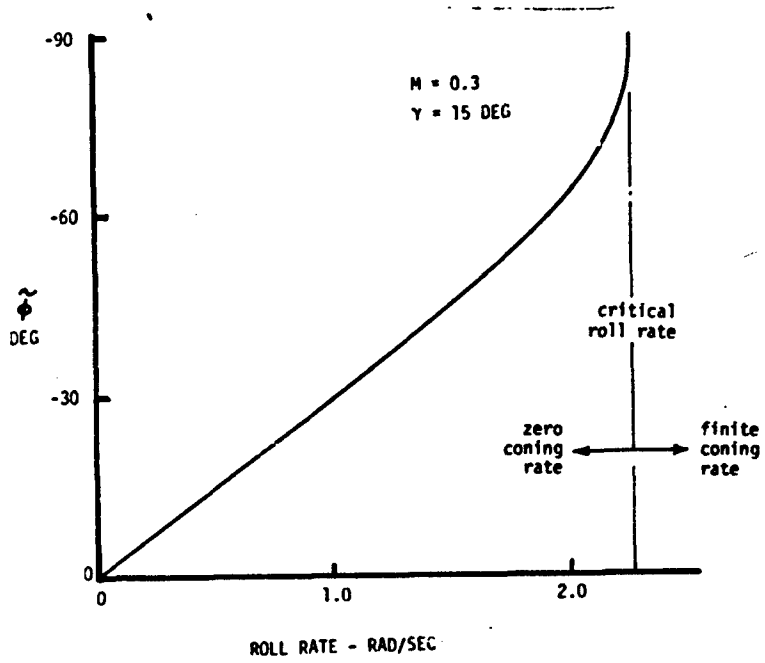

Figure 4. Variation of Angle of Attack Plane Orientation with Roll Rate for S-Curve Bomblet

A significant result, as can be seen from Figure 5, is that as the roll rate decreases to zero the solutions for ϕ also approach zero. In the limiting case of zero roll rate the bomblet continually flies nose up with the lift vertical. Further analysis of Equation (2) shows that for positive roll and positive Magnus the nose of the bomblet points to the left of the velocity vector (as viewed looking in the direction of flight). Similarly, the nose of the bomblet points to the right when the magnus moment is negative.

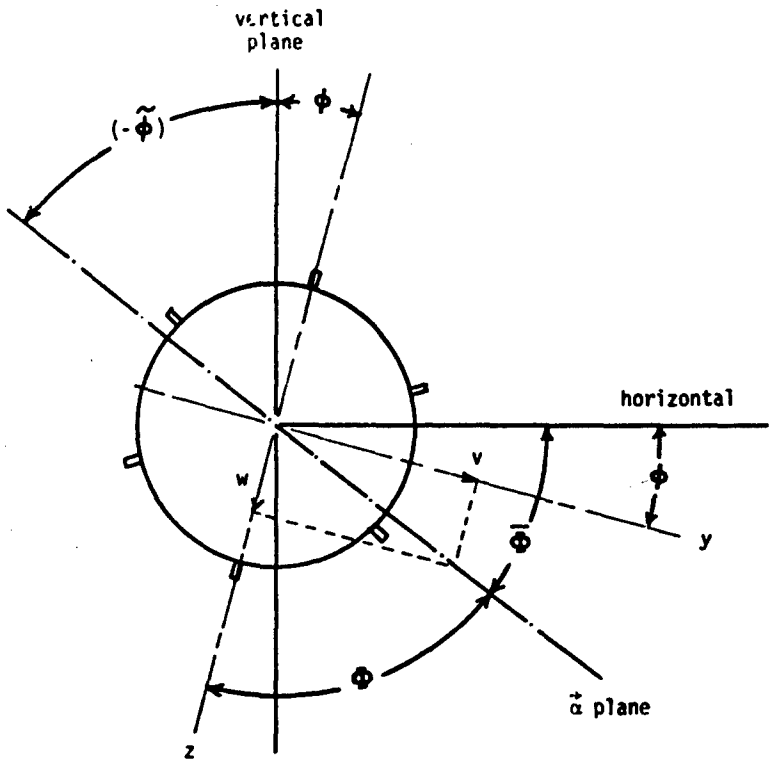

Figure 5. Description of Angle of Attack Plane Orientation and Aerodynamic Roll Angle

To confirm that the steady-state solutions are indeed stable solutions (i.e., that any oscillation, $\Delta\tilde{\phi}$, is damped) a perturbation differential equation is written using $\Delta\tilde{\phi}$ as the dependent variable. Analysis of the perturbation equation shows that stable solutions exist only for $-\pi/2 < \tilde{\phi} < \Pi/2$. Outside this region the $\Delta\tilde{\phi}$ perturbations are unstable. This implies that the nose of the bomblet is always nose-up with respect to the trajectory when stable zero-coning solutions exist.

Now, consider the case where the classical spin dependent magnus moment is negligible and the side moment C_{SM} is present. Equation (4) implies a maximum for C_{SM} irrespective of the trim angle of attack.

Consider also the effect of C_{SM}, when C_{SM} is a harmonic function of the aerodynamic roll angle, Φ. This functional relationship exists for most finned bodies. A general solution in the form of Equation (1) is not readily attainable because of the complex relationship between $\tilde{\phi}$ and Φ. However, the special case where $p = \phi = 0$ is worthy of examination, since then $\tilde{\phi} = -\Phi$. We can rewrite the contribution of C_{SM} (Φ) as

$$\frac{dC_{SM}}{d\Phi} \quad \Delta\tilde{\phi}$$

when the bomblet symmetry planes are approximately aligned with the angle of the attack plane.

Examination of the stability criteria for perturbations $\Delta\tilde{\phi}$ about $\tilde{\phi}$ = constant[1] shows that for stable solutions

$$\frac{dC_{SM}}{d\Phi} > 0 \qquad (5)$$

In other words, the angle of attack plane will rotate until Φ attains a value where relationship (5) is satisfied. Six-degrees-of-freedom motion computations show that inequality (5) is valid even when the spin rate is finite.

Six-Degrees-of-Freedom Motion Simulations. Six-degrees-of-freedom simulations have been used to verify the zero coning theory, to examine the initial transient motion, and to assess the effect of the highly nonlinear aerodynamic coefficients. These simulations were accomplished for the cylindrical afterbody S-Curve bomblet configurations (Figure 1-a and Table I) using a special six-degrees-of freedom trajectory program. (10) The dispenser event conditions are typical of subsonic aircraft weapons delivery.

TABLE I. ASSUMED PHYSICAL CHARACTERISTICS OF S-CURVE AND ROLL-THROUGH-ZERO BOMBLETS

Body diameter	- 2 inches
Body length	- 8 inches
Weight	- 1.51 pounds
I_x	- 1.629×10^{-4} slug-ft^2
I	- 1.06×10^{-3} slug-ft^2

[1] For six fins, $\tilde{\phi}$ = 0, $\pi/6$, $\pi/3$, 2 $\pi/3$, etc.

A comparison of the six-degrees-of-freedom motion with that predicted by the zero coning theory is illustrated in Figure 6. The coning motion is represented by the variable, $\bar{\Phi}$, which represents the orientation of the angle of attack plane with respect to horizontal (Figure 5). Several arbitrary initial orientations of the angle of attack plane are assumed for the six-degrees-of-freedom motion calculations. The initial angle of attack is 5 degrees. For these calculations only the spin dependent Magnus moment is assumed to be present (original estimate curve of 3), and the fin cant is 0.02 degree . This cant angle results in a steady-state roll rate less than the predicted critical roll rate.

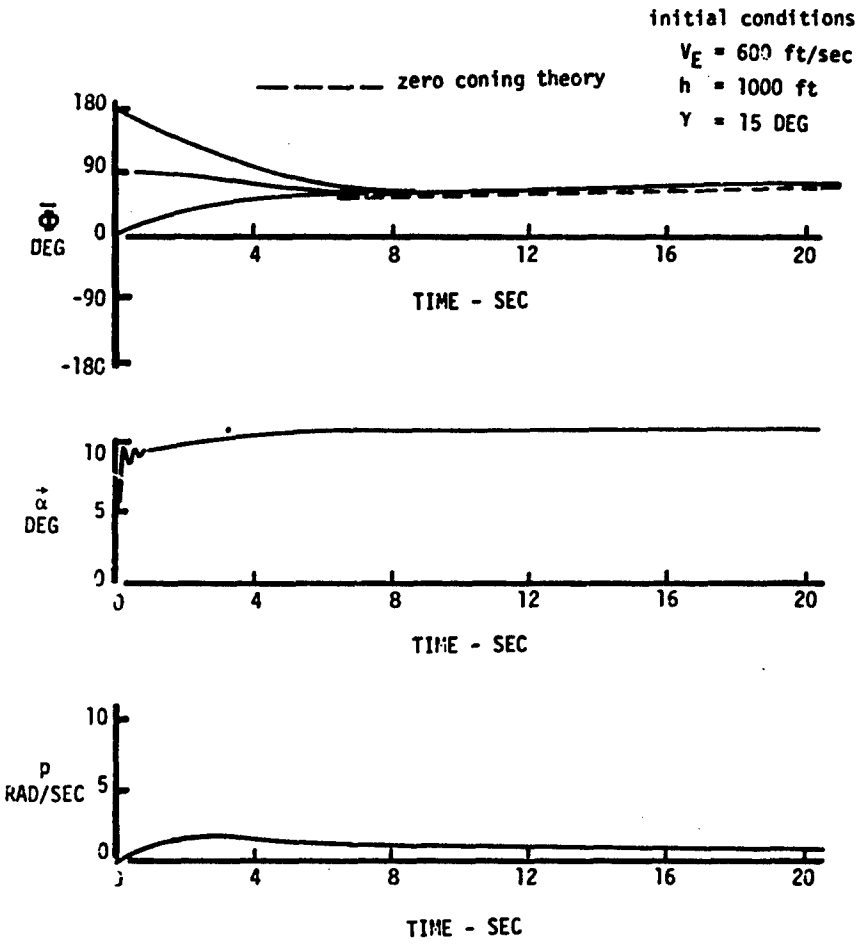

Figure 6. Motion Histories for S-Curve Bomblet with 0.02 Degree Fin Cant

As can be seen from the $\bar{\Phi}$ motion history, the angle of attack plane converges to a fixed orientation after about six seconds of flight, regardless of the initial orientation. The steady-state value of $\bar{\Phi}$ closely approaches the theoretical zero-coning solution. Note that the angle of attack rapidly approaches the nominal trim angle of attack and that the transient motion is heavily damped.

With an increase in the cant angle to 0.1 degree, the angle $\bar{\Phi}$ does not approach a steady-state value, but continues to increase, negatively. Figure 7 illustrates this motion, which can be compared directly with the results for the smaller cant angle. Although for this case the coning rate is finite, nonetheless, the coning rate is only about 6 percent of the roll rate.

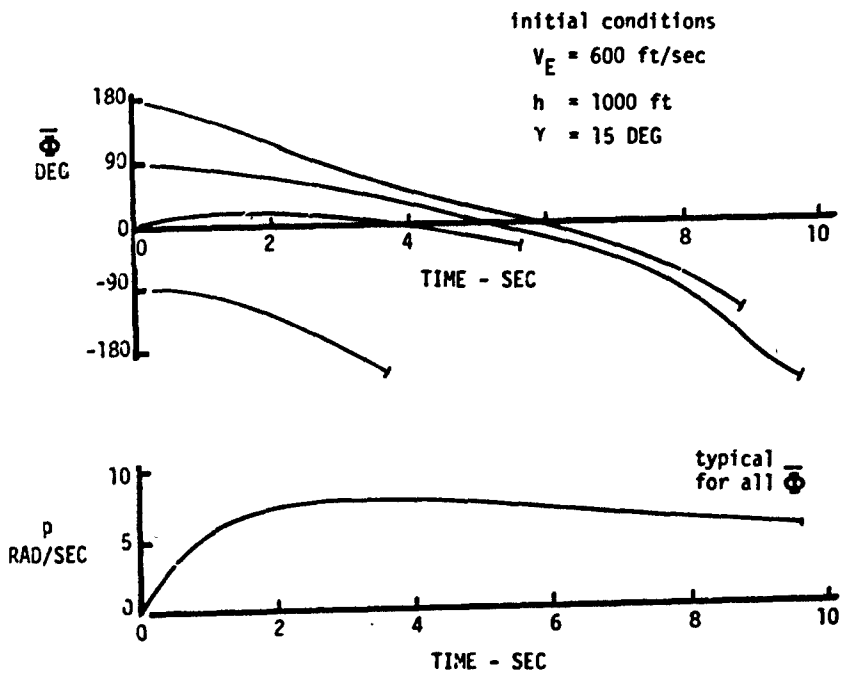

Figure 7. Motion Histories for S-Curve Bomblet with 0.1 Degree Fin Cant

When the aerodynamic coefficients are modified to include roll angle dependency (and fin-body lateral misalignment and static unbalance are also introduced) the bomblet dynamics become very complicated. For example, when the moment vector representing the lateral misalignment is aligned with the angle of attack plane, this moment acts like a magnus moment and tends to cause coning. Interestingly, this effect becomes more pronounced as the roll rate due to fin cant is decreased.

Roll torques due to static unbalance, fin cant, and the effect of aerodynamic roll angle on the fins, as well as the side moment, can contribute to anomalous rolling motions and roll lock-in conditions. Thirty-five trajectories and motion histories were computed using the subsonic dispenser event conditions given to Table II and the following bomblet asymmetries:

Fin cant	= 0.1 degree (constant)
Lateral misalignment	= 0.3 degree (standard deviation)
Static unbalance	= 0.0016 inch (standard deviation)

TABLE II. EVENT CONDITIONS FOR REPRESENTATIVE DISPENSER FUNCTION

Subsonic Delivery

V_E = 900 ft/sec
γ = 45 deg
h(HOB) = 2000 ft

Transonic Delivery

V_E = 1145 ft/sec
γ = 65.7 deg
h(HOB) = 2000 ft

Supersonic Delivery

V_E = 2000 ft/sec
γ = 50 deg
h(HOB) = 2000 ft

Random values for the initial angular orientation of the angle of attack plane, fin symmetry planes, static unbalance, lateral misalignment, and initial pitch disturbance were selected. Out of the thirty-five trajectories, twenty-one developed a roll lock-in type motion with Φ constant, while for the remainder Φ varied continuously. For those that locked-in, the lock-in angles are plotted in Figure 8, along with the variation of the side moment with Φ. As can be seen, lock-in occurs only when the gradient of the side moment is positive.

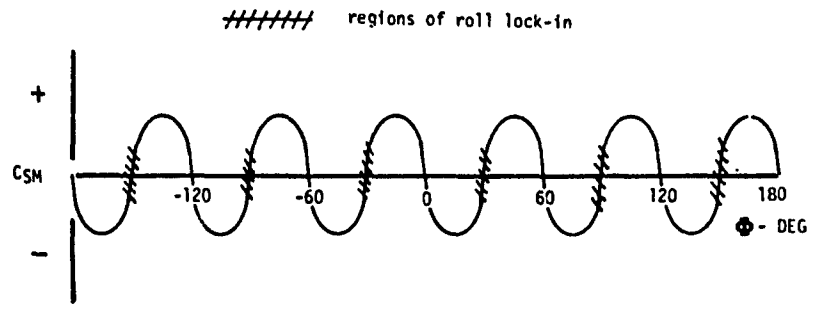

Figure 8. S-Curve Bomblet Roll Lock-in Characteristics

With zero fin cant the percentage of those bomblets experiencing lock-in increased to 100 percent, while for 0.5 degree cant no lock-ins were encountered. Further note should be made of the fact that when lock-in occurred, the angle of attack remained well behaved, and for the configurations considered, there was no noticeable tendency for the trim angle of attack to increase.

While the flight dynamics of the S-Curve type bomblet must be reasonably well behaved, the essential requirement is the achievement of a large and reasonably uniform dispersion pattern. Thus, the integrated effect of the motion, as related to the deflection of the bomblet trajectories is the only thing that really matters. Also, even though large dispersions are desired, some bomblets with poor dispersion can be accepted as a means of filling the center of the pattern. This leads one to consider the dispersion from a purely statistical point of view. The Monte Carlo method is well suited to this type of problem and its use for dispenser prediction is described in a subsequent section.

Roll-Through-Zero Bomblet

Aerodynamic Design Considerations. The aerodynamic design of a roll-through-zero-type bomblet with large body-fixed trimmed lift would appear straightforward. A means must be provided for trimming the bomblet to a large angle of attack, and a small roll torque must be introduced to reverse the initial rolling motion of the bomblet. Unfortunately, the means provided for trimming the bomblet can often lead to sizeable roll and side moments which are dependent upon the roll orientation of the bomblet. Thus, under transient motion conditions, such as occur immediately after dispenser opening, these induced moments can completely overpower the small roll torque introduced for reversing the roll.

Six-degrees-of-freedom motion studies of a high-lift bomblet configuration with small wing-like surfaces, which had large roll dependent

moments, showed that this type of bomblet has very erratic roll motion and poor dispersion. Consequently, an alternate bomblet concept similar in external geometry to the S-curve bomblet (Figure 1c) was selected for investigation. Two of the fins are given an incidence of 10 degrees for the purpose of trimming the bomblet to a finite angle of attack.

Figure 9 illustrates the aerodynamic characteristics of the bomblet as a function of angle of attack with the bomblet in the trimmed roll orientation. The variations of the coefficients with roll are depicted in Figure 10. The variations of the forces and moments with roll are sizeable but less than those of the original high-lift configuration. The loss of lift due to the aft placement of the aerodynamic trim surfaces is apparent.

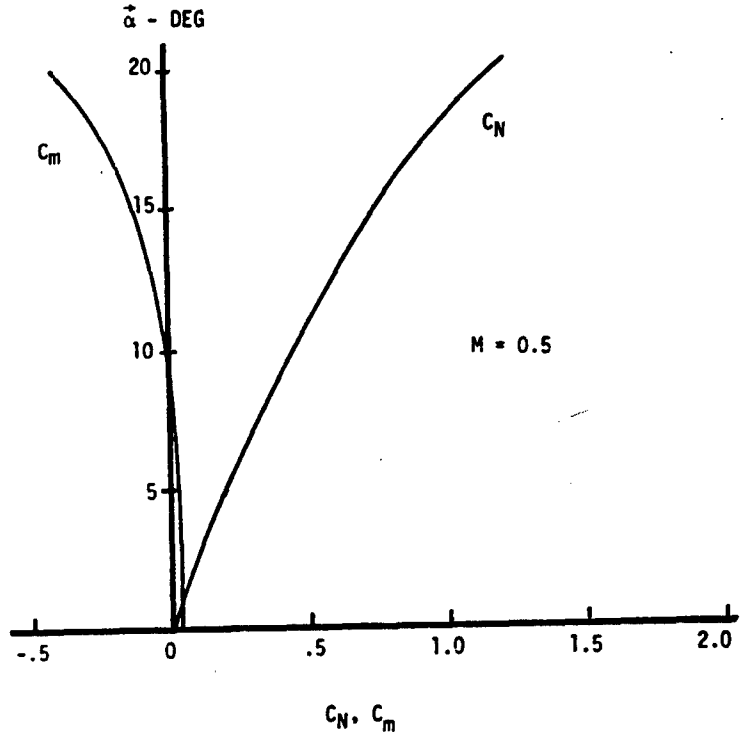

Figure 9. Roll-Through Zero Bomblet Aerodynamic Characteristics as a Function of Angle of Attack (Trimmed Roll Orientation)

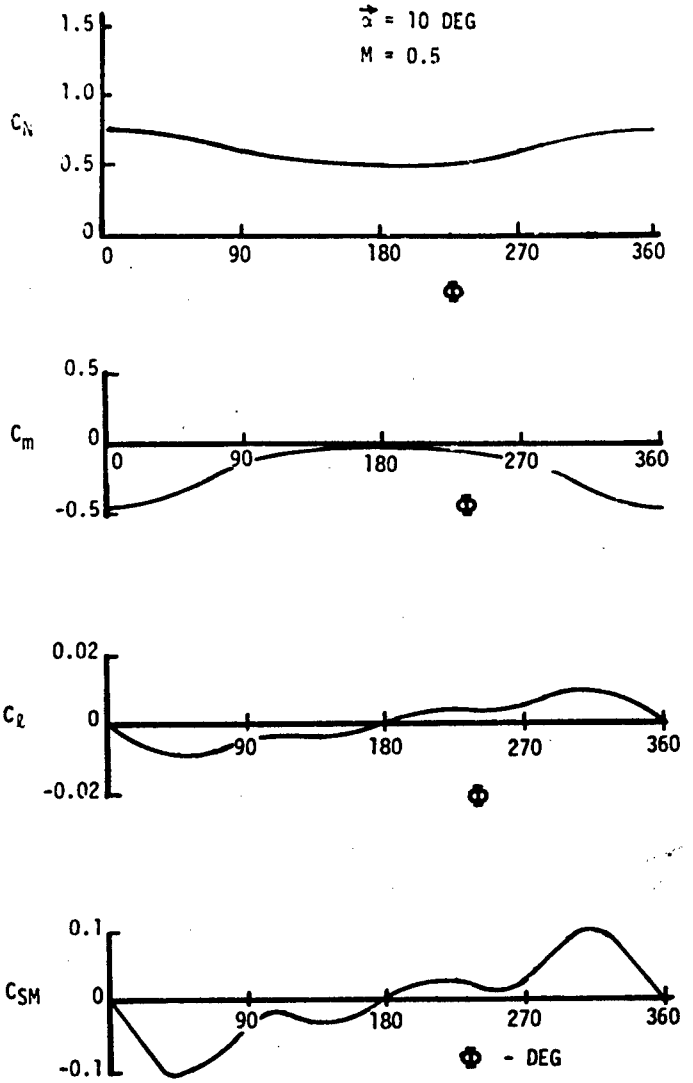

Figure 10. Effect of Aerodynamic Roll Angle on Aerodynamic of Roll-Through-Zero Bomblet

Particularly noteworthy from Figure 10 is the fact that the gradient of the roll torque with respect to the aerodynamic roll angle at the trim orientation is positive or unstable. Also note that the side moment gradient is positive. The latter has a very significant stabilizing influence on the aerodynamic roll angle by nature of the fact that the coning motion induced by C_{SM} tends to return the aerodynamic roll angle to the trim orientation. This stabilizing effect would become destabilizing if the aerodynamic surfaces used for trim were placed forward of the center of gravity.

Simplified Motion Theory. A simplified closed-form solution is readily obtained for the motion of a roll-through-zero-type bomblet during its dispersal phase of flight. If induced aerodynamic effects are neglected and we assume constant velocity, linear aerodynamics, a constant roll torque coefficient, C_{ℓ_o}, and trimmed flight, the solution of equations-of-motion for the roll and lateral translation degrees-of-freedom from the time at which $p = 0$ to time $\hat{t} = x$ is

$$\frac{y_e' + i\, z_e'}{d} = \frac{C_{N_T}}{2m'} \sqrt{\frac{2\pi\ I_x'}{C_{\ell_o}}}\ C(x) + i\, S(x) \qquad (6)$$

where $C(x)$ and $S(x)$ are Fresnel integrals

$$C(x) = \int_0^x \cos\left(\frac{\pi u^2}{2}\right) du$$

$$S(x) = \int_0^x \sin\left(\frac{\pi u^2}{2}\right) du$$

and $$x = \sqrt{\frac{2\phi}{\pi}}$$

The Fresnel integrals have asymptotic values for $\phi \to \infty$

$$C(x) = \frac{1}{2}$$

$$S(x) = \frac{1}{2}$$

such that

$$\left|C(x) + i\, S(x)\right| = \sqrt{\frac{1}{2}} \qquad (7)$$

The same result as equation (7) is approximated by $\phi = \pi/4$, where

$$\left| C\left(\frac{1}{\sqrt{2}}\right) + iS\left(\frac{1}{\sqrt{2}}\right) \right| \simeq \frac{1}{\sqrt{2}} \tag{8}$$

Therefore, starting from zero roll rate, the lateral deflection of the trajectory after rolling through an angle $\phi = \pi/4$ is nearly identical to the deflection which would occur after a large number of roll cycles. If roll-through-zero occurs and there exists at least one-eighth of a roll cycle before and after the roll-rate reversal, then the total deflection of the trajectory is approximated by

$$\Delta\gamma = \frac{y_e' + i\, z_e'}{d} = 2\left(\frac{C_N}{2m'}\right)\sqrt{\frac{2\pi\, I_x'}{C_{\ell_o}}}\left(\frac{1}{\sqrt{2}}\right) = \frac{C_N}{2m'}\sqrt{\frac{\pi\, I_x'}{C_{\ell_o}}} \tag{9}$$

An important result obtained from the above relationship is that very large trajectory deflections can be achieved, provided that a small roll torque is used to de-spin the bomblet.

An estimate of the dispersion at ground level can easily be made, if the bomblet has a large ballistic coefficient such that the flight path following roll-through-zero is relatively straight. The along-range and cross-range dispersions (R and r, respectively) due to $\Delta\gamma$ are simply

$$R = \frac{h}{\sin^2\gamma}\,\Delta\gamma \tag{10}$$

$$r = \frac{h}{\sin\gamma}\,\Delta\gamma \tag{11}$$

Six-Degrees-of-Freedom Motion Simulations. Figure 11 illustrates a typical set of motion histories for the roll-through-zero bomblet, based on the subsonic event conditions of Table II. The data are selected from one of a series of trajectories comprising a Monte Carlo dispersion study. This particular bomblet has an initial negative roll rate of 1.0 rps, a mean effective fin cant of 0.115 degree, and a cg lateral offset of 0.001 inch.[2]

[2]It is to be noted that for this particular bomblet the maximum induced roll moment due to cg offset is about 60 percent of that due to the intentional fin cant.

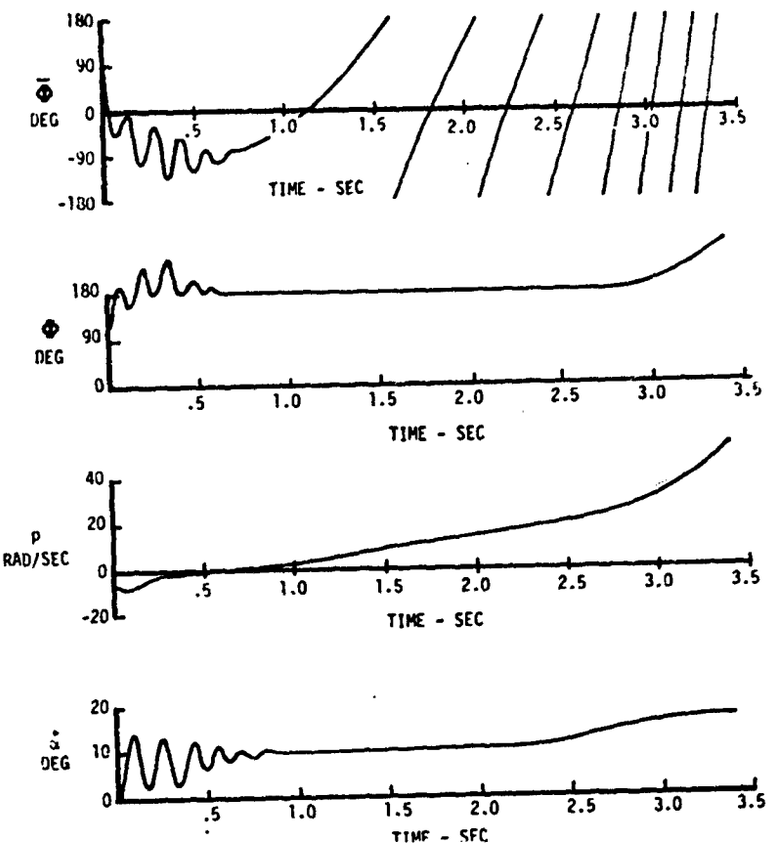

Figure 11. Motion Histories for Roll-Through-Zero Bomblet

Examination of Figure 11 shows that about 0.5 second is required for the bomblet to attain zero roll rate and for the aerodynamic roll angle, Φ, to stabilize at the trim orientation, $\Phi \approx \pi$. The spacial orientation of the angle of attack plane, angle $\bar{\Phi}$, remains approximately within one quadrant during the first 1.0 second of flight, and this is the period during which the trajectory is deflected. The trim orientation remains stable at $\Phi = \pi$ for approximately 3.0 seconds of flight (thus substantiating that the roll torque need not be stable), but subsequently the spin rate approaches the resonance spin rate and the familiar phase shift in the trim orientation begins to occur.

The lateral cg offset is a very critical factor for the roll-through-zero-type bomblet. Because the aerodynamic roll angle under trim conditions is nearly invariant, the induced roll torque due to cg offset results in random variations in roll torque and roll rate. If these become large, the roll rate builds up to values which approach or exceed the pitch

resonance frequency. Then the trim phase shift causes the side moment to increase with possible adverse effect on the dynamic stability such that very large coning angles ensue.

These considerations complicate the aerodynamic design since, if the designer attempts to increase the pitch frequency to provide more lateral cg tolerance, the trim moment requirements also tend to increase. This, in turn, leads to increased induced aerodynamic moments from the larger trim surfaces.

SECTION III

MONTE CARLO DISPERSION PREDICTION

Procedure

The motion of an actual S-Curve bomblet or roll-through-zero bomblet differs considerably from that of an ideal bomblet due to configurational asymmetries and departures from complete rotational symmetry. In addition, the initial motion imparted to the bomblets at dispenser opening and during the subsequent period of cluster breakup tends to be stochastic in nature.

The Monte Carlo method provides a means for ascertaining the dispersion characteristics of a bomblet cluster by computation of the probable motion and impact points of a large number of bomblets. This was accomplished by the use of statistical values for the initial motion parameters and bomblet configurational asymmetries. For each simulated dispenser event, from 30 to as many as 100 six-degree-of-freedom trajectories are computed to determine the probable dispersion and impact pattern of the bomblet cluster.

The Monte Carlo simulations described in this report have been computed primarily for the representative subsonic dispenser event conditions described in Table II. The bomblet physical parameters correspond to the data of Table I. The bomblet size and inertial properties are representative of a hypothetical configuration.

Initial Motion Parameters

The initial motion parameters are evaluated in accordance with the probable time of break-out from the cluster, defined as t_{b_o}. At this instant the bomblet is no longer influenced by the multi-component flow effects which exist because of bomblet-bomblet and bomblet-dispenser interference effects. The statistical values of the motion parameters at break-out are determined empirically from flight test data or suitable assumptions.

The probable cluster break-out time is established using a special distribution function. Figure 12 shows a typical curve of cumulative frequency versus cluster break-out time based on experimental data.

The bomblet velocity at t_{b_o} is assumed to be comprised of two components: a component in the mean direction of motion of the cluster, and a radial velocity component, with a Gaussian magnitude (but not necessarily zero mean) and uniformly random orientation. The longitudinal component of velocity depends upon the event velocity and the cluster deceleration. The bomblet cross-angular velocity is assumed to be Gaussian in magnitude and uniformly random in direction. The initial angle of attack is arbitrarily selected as zero because the cross-angular velocity establishes the magnitude of the first oscillation peak.

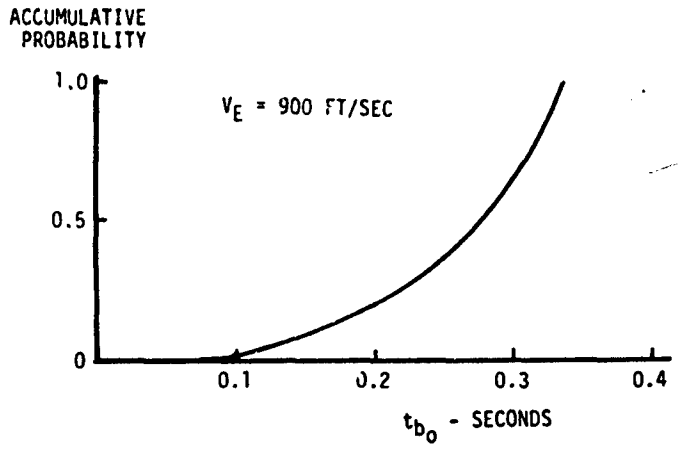

Figure 12. Statistics of Bomblet Cluster Breakup

For the subsonic event conditions given in Table II, the standard deviations for the initial radial velocity and initial cross-angular velocity are

$$V_R = 20 \text{ ft/sec}$$

$$q^* = 35 \text{ rad/sec}$$

Configurational Asymmetries

The physical variations in bomblet configuration considered in the present Monte Carlo simulations are fin cant, longitudinal misalignment, and lateral cg offset. The latter two parameters are considered to be Gaussian in magnitude and uniformly random in orientation. In general, the fin cant has a non-zero mean and Gaussian distribution. Since there are no S-Curve or roll-through-zero bomblets in production, estimates for the configurational asymmetries are based on other representative ordnance.

Values for the standard deviations of fin cant error, longitudinal misalignment and lateral cg offset are selected on the basis of fabrication accuracies which are representative of small ordnance. Of these, the standard deviation of cg lateral offset is most sensitive to the particular fabrication and loading techniques used.

For most of the Monte Carlo simulations the standard deviation of cg lateral offset is 0.0016 inch, although a value as large as 0.0400 inch is considered for the S-Curve bomblet.

The standard deviation value for effective fin cant error is dependent upon the number of fins since, if the variance of all the fins is identical, the standard deviation of roll torque is

$$\text{standard deviation } C_{\ell} = \frac{C_{\ell_\delta}\ \sigma_F}{\sqrt{n}}$$

where σ_F is the standard deviation of error of a single fin. For a six-fin configuration, the standard deviation of effective cant, δ_{eff}, is $\delta_{eff} = 0.41\ \sigma_F$. The effective longitudinal misalignment of the fin assembly is similarly defined by $C_N = C_{N_\delta}\ \delta_{eff}$. For six-fins and neglecting fin-fin interference, the standard deviation of δ_{eff} for longitudinal misalignment is $\delta_{eff} = 1.12\ \sigma_F$. This is combined with the body misalignment on an RSS basis. In the present studies a value of 0.2 degree is used for both σ_F and the standard deviation of body misalignment, based on an averaging of several data sources.

SECTION IV

MONTE CARLO IMPACT-DISPERSION PATTERNS

S-Curve Bomblet

A computed Monte Carlo dispersion pattern for the type a S-Curve bomblet configuration is depicted in Figure 13. For this simulation, the bomblets have a mean fin cant of zero degrees, and a standard deviation of cg lateral offset of 0.0016 inch.

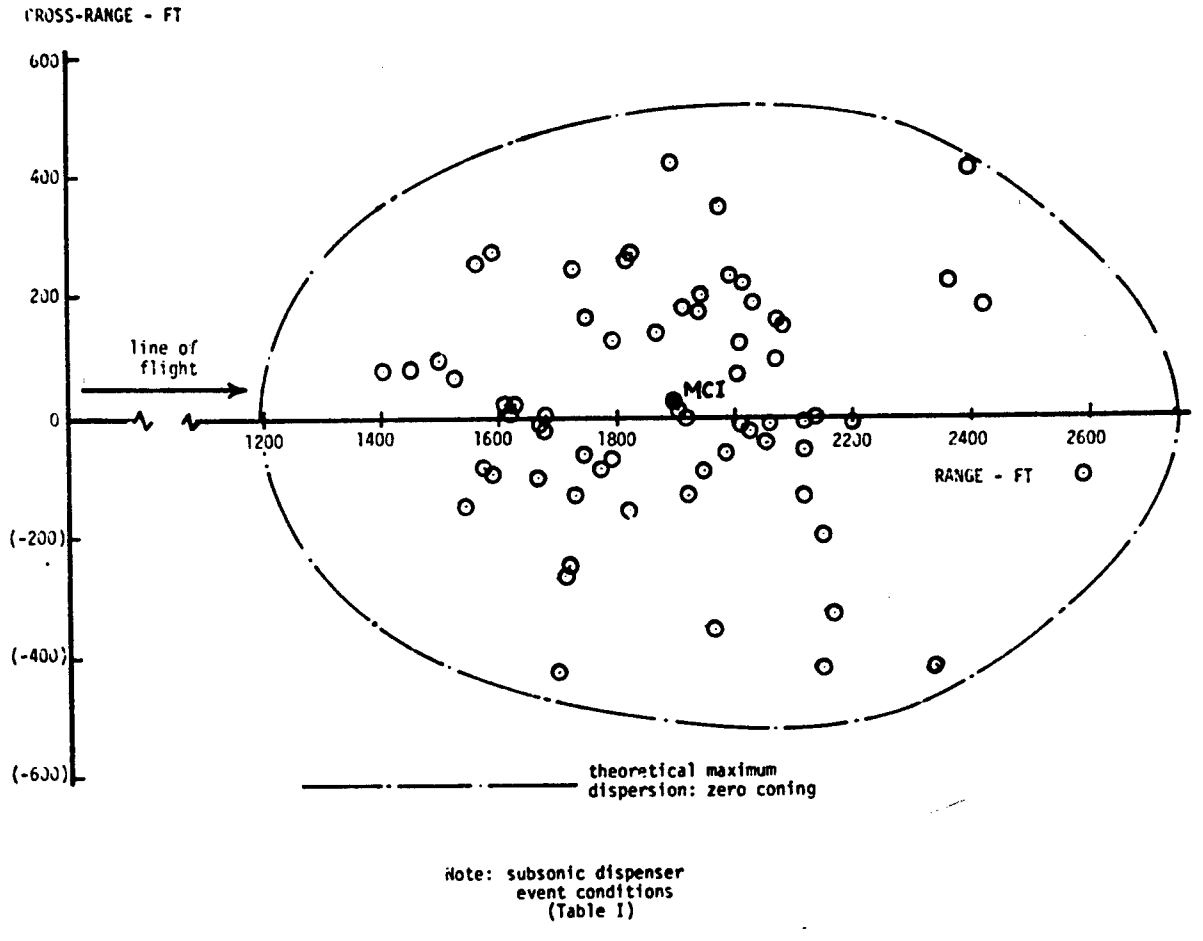

Figure 13. Monte Carlo Impact-Dispersion Pattern for S-Curve Bomblet

Statistical analysis of the impact pattern shows that the standard deviations of along-range and cross-range dispersion, with respect to the mean center-of-impact, are ± 246 feet and ± 185 feet, respectively.

The maximum dispersion is about 2.3 times greater than the standard deviation values, which emphasizes the fact that the impact points are concentrated toward the center of the pattern.

Accuracy. To obtain an approximate indication of the impact pattern statistical repeatability, a set of 33 trajectories was rerun several times using the same statistical distribution functions but with different random numbers. It was determined that for a Monte Carlo sample size corresponding to 33 trajectories, the standard deviations of along-range and cross-range dispersion are accurate to within about ±25 feet at the 90 percent confidence level.

Comparison with Theory. A theoretical dispersion boundary is plotted in Figure 13 for purposes of comparison with the Monte Carlo results. The theoretical boundary represents the dispersion which would be achieved with zero coning. In determining the zero coning boundary, an average time for cluster-breakout was assumed. As can be seen, several impact points approach the zero-coning boundary, and this number would be expected to increase in proportion to the total number of trajectories simulated. Thus, the zero coning theory provides a close approximation of maximum pattern size.

Effect of Static Unbalance. Monte Carlo impact patterns have been computed for various arbitrary values of the standard deviation of lateral cg offset. The trend of the maximum dispersion and the standard deviation of dispersion with the standard deviation of lateral cg offset is depicted in Figure 14. There is a decrease in both the maximum and standard deviation values of dispersion with increasing cg offset. The data show that a cg offset tolerance of 0.01 inch can be applied, if a 10 percent reduction in cross-range dispersion can be accepted. It should be noted that the sensitivity to static unbalance increases appreciably when a larger trim angle of attack is selected.

Effect of Fin Cant. It has been theorized that the coning motion due to the body-fixed roll-dependent side moments would be less if an intentional roll rate was introduced such that the effect of these moments on the flight path would tend to be averaged. Dispersion patterns were computed with a mean fin cant of 0.5 degree for a range of static unbalance. The results are compared with the zero cant data in Figure 15. With the intentional cant angle, there is a large increase in the standard deviation values of along-range and cross-range dispersion, thus proving the effectiveness of this bomblet modification.

Effect of Initial Motion Parameters. The sensitivity of the S-Curve bomblets to the magnitude of the initial motion disturbance has been investigated using the Monte Carlo method. Doubling the initial tumble rate to 70 rad/sec had negligible effect on the dispersion, even though the magnitude of the first oscillation peak was as large as 90 degrees.

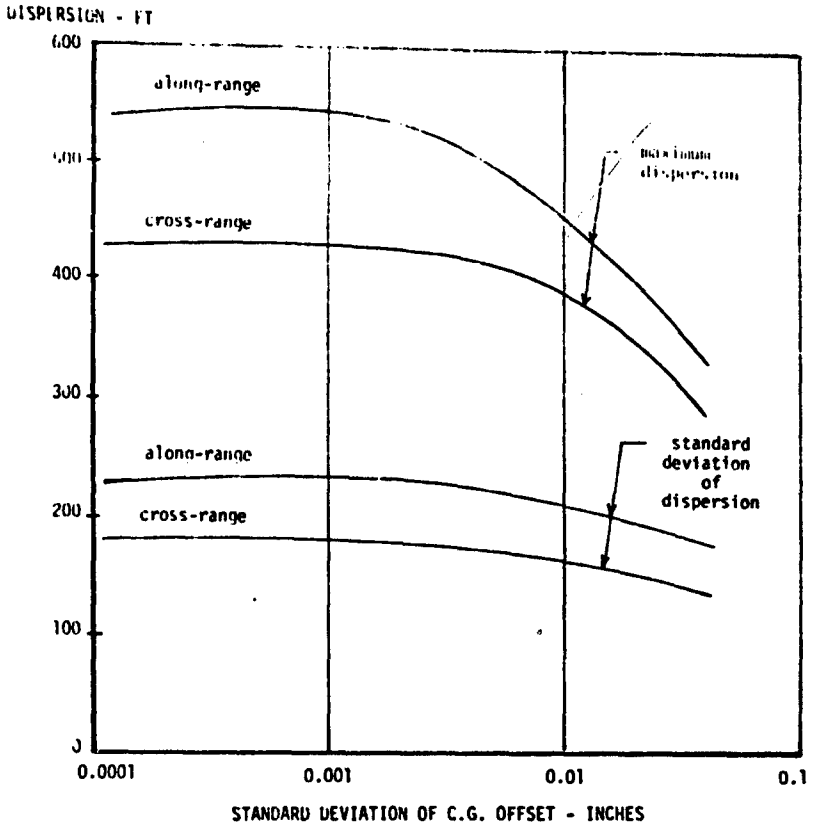

Figure 14. Effect of Static Mass Unbalance on S-Curve Bomblet Dispersion (Monte Carlo Results)

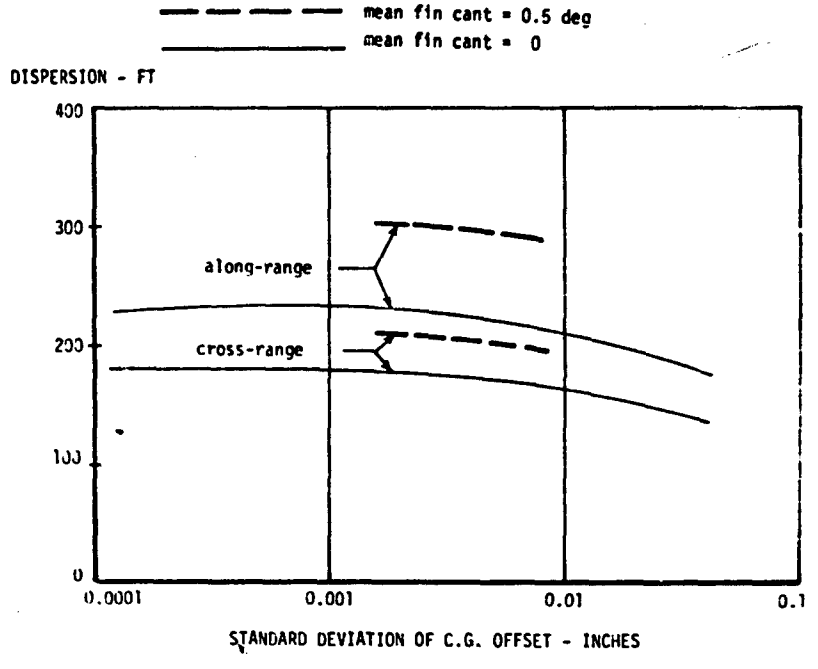

Figure 15. Effect of Mean Fin Cant Angle on S-Curve Bomblet Dispersion (Monte Carlo Results)

Effect of Increasing Trim Angle of Attack. Increasing the bomblet nominal trim angle of attack from 10 degrees to 16 degrees resulted in a dispersion increase (standard deviation) nearly proportional to the ratio of trim lift coefficient. These results were achieved in spite of the increased nonlinearity of the aerodynamic coefficients at the larger angle of attack.

Transonic and Supersonic Event Conditions. For transonic delivery conditions, calculations have shown the boattail afterbody configuration (Figure 1b) to have more desirable dispersion characteristics than the cylindrical afterbody bomblet, even though the trim angle of attack is less than that of the cylindrical afterbody for Mach numbers between 1.0 and 1.5. Monte Carlo dispersion data for the boattail afterbody bomblet are summarized in Table III for the representative transonic and supersonic event conditions as given in Table II.

TABLE III. TRANSONIC AND SUPERSONIC DISPERSION CHARACTERISTICS OF S-CURVE BOMBLET WITH BOATTAIL AFTERBODY

	Standard Deviation Range Dispersion (Feet)	Standard Deviation Cross-Range Dispersion (Feet)
Transonic Event	202	183
Supersonic Event	959	470

For transonic delivery, the impact dispersion is comparable to that for the cylindrical afterbody bomblet delivered at high subsonic velocity. In contrast, for supersonic delivery, the range dispersion is increased by a factor greater than four and the cross-range by a factor greater than two.

Roll-Through-Zero Bomblet

A Monte Carlo dispersion pattern for the roll-through-zero type is illustrated in Figure 16. The standard deviation values of range and cross-range dispersion are 207 feet and 159 feet, respectively. The dispersion pattern has a maximum diameter of about 650 feet. For this simulation the standard deviation of bomblet static unbalance is 0.0016 inch.

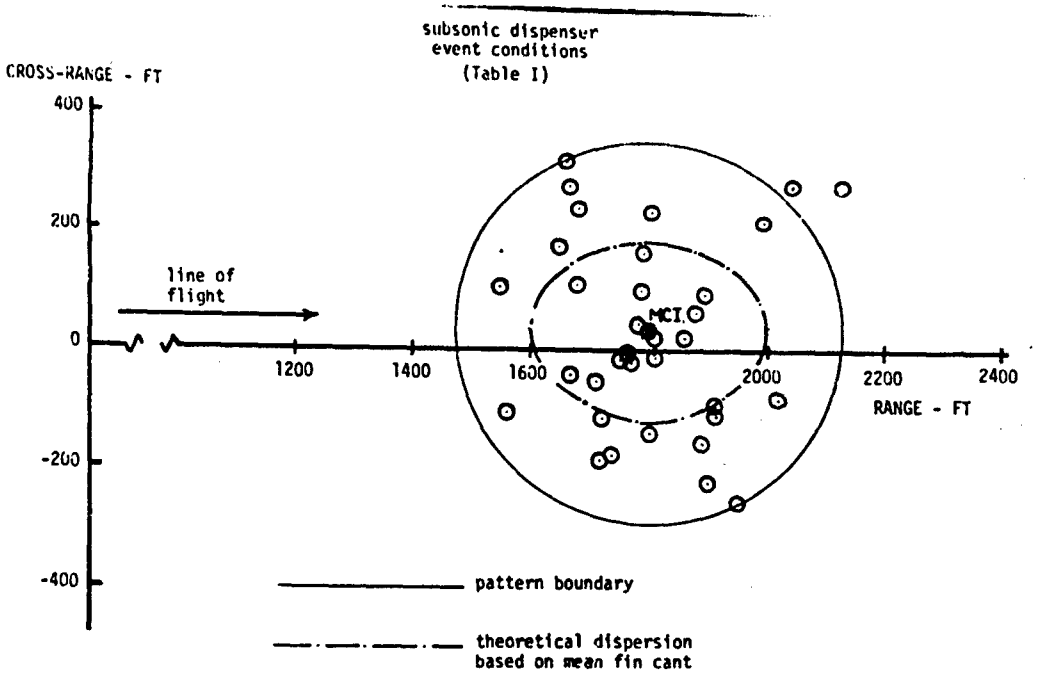

Figure 16. Monte Carlo Impact Dispersion Pattern for Roll-Through-Zero Bomblet

Comparison with Theory. Figure 16 also depicts the theoretical dispersion boundary obtained using equations (9), (10), and (11) with the roll torque coefficient in equation (9) corresponding to the mean fin cant angle. There is excellent agreement between the theoretical dispersion boundary and the standard deviations of range and cross-range dispersion computed from the Monte Carlo impact pattern. However, using the mean fin cant angle, the maximum dispersion is significantly underpredicted, as would be expected.

Comparison with S-Curve. A comparison of the impact pattern data for the S-Curve and roll-through-zero bomblets (standard subsonic event conditions) shows that the ratios of the standard deviation values of dispersion for the two types of bomblets are very nearly proportional to the respective trimmed lift coefficients. This comparison is based on an S-Curve bomblet configuration with zero mean fin cant. For supersonic event conditions, the performance of the roll-through-zero bomblet is poor compared to the S-Curve bomblet, because the roll-through-zero bomblet dispersion does not benefit from increased dynamic pressure.[3]

[3] Equation (9) shows that, theoretically, the roll-through-zero bomblet dispersion is independent of velocity.

SECTION V

COMPARISON OF S-CURVE AND MAGNUS ROTOR BOMBLETS

One of the advantages of the S-Curve-type bomblets is that the aerodynamic dispersal force is generated immediately upon bomblet ejection into the air stream. Further, the dynamic pressure is large during the initial phase of flight and this aids in the rapid dispersal of the bomblet cluster. In contrast, Magnus rotor bomblets must undergo a period of spin-up during which the aerodynamic lift is small. The lift will remain small until the magnus rotor decelerates to below approximately 0.5 Mach number.

Figure 17 compares typical S-Curve and magnus rotor trajectories for the representative subsonic dispenser event conditions of Table II. The more rapid dispersion of the S-Curve-type bomblet is clearly evident. The better performance of the S-Curve-type bomblet can also be translated into a lower height of burst (HOB). For example, assuming the same impact dispersion, the S-Curve bomblets can be deployed at a 650-foot lower altitude.

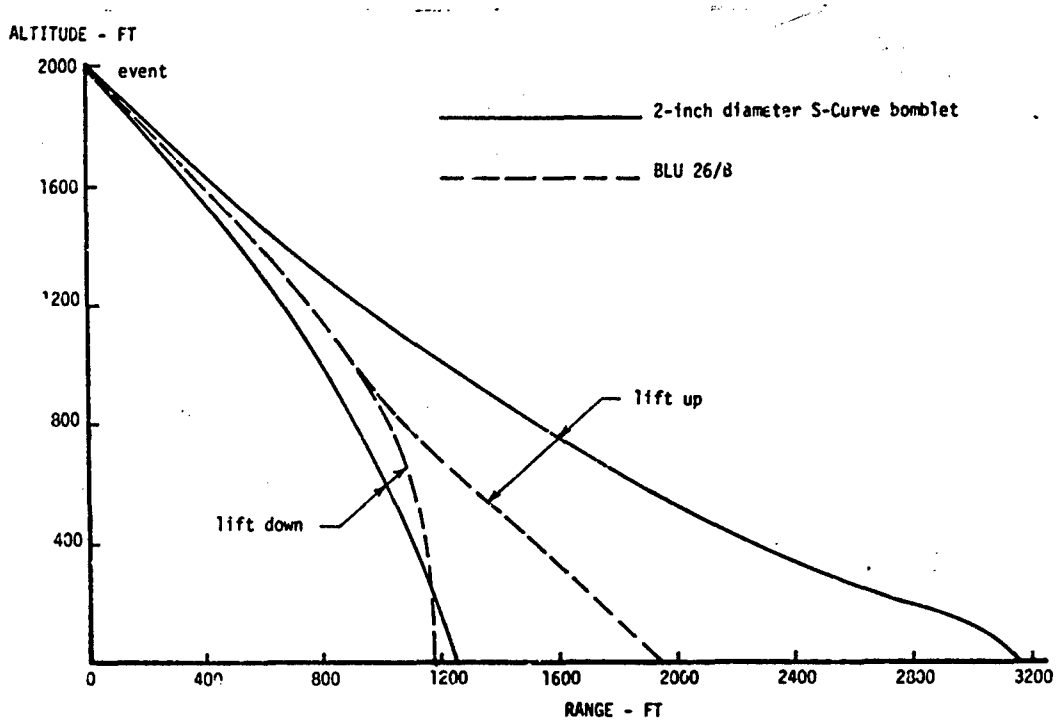

Figure 17. Comparison of S-Curve Bomblet and Magnus Rotor Trajectories

SECTION VI

CONCLUSIONS

On the basis of analytical studies, including Monte Carlo impact dispersion predictions, both the S-Curve and roll-through-zero-type bomblets are found to have good potential for cluster dispenser and cluster warhead applications. These bomblets must be very carefully designed to insure that the proper aerodynamic characteristics are obtained and attention must be given to the allowable configurational asymmetries.

REFERENCES

1. Merchant, D.G. and R. L. Pope, "The Scattering of Bomblets by an Aerodynamic Method," Australian Defence Scientific Service, Weapons Research Establishment, Technical Note HSA 126, October 1967 (Confidential).

2. Burke, Lawrence R., Jr., "R/V Roll Trim Statistical Analysis Technique", Third Technical Workshop on Dynamic Stability, Ames Research Center, November 4 - 7, 1968.

3. Shadow, T.O., "Wind Tunnel Investigation of the Transonic Static Stability Characteristics of Three Bomblet Munition Models Used in the Evaluation of Aerodynamic Dispersion Techniques," Arnold Engineering Development Center Report No. AEDC-TR-70-233, September 1970.

4. Uselton, Bob, Jack Carman and Tom Shadow, "Dynamic Stability Characteristics of Axisymmetric Bomblet Munition Models at Mach Numbers 0.3 through 1.2," Arnold Engineering Development Center Report No. AEDC-TR-70-270, December 1970.

5. Carman, J.B., B. L. Uselton, and C.E. Burt, "Roll-Damping, Static Stability, and Damping-In-Pitch Characteristics of Axisymmetric Bomblet Munition Models at Supersonic Mach Numbers," Arnold Engineering Development Center Report No. AEDC-TR-71-88, April 1971.

6. Shadow, T. O., "Transonic Roll-Damping and Magnus Characteristics of Three Bomblet Munition Models Used in the Evaluation of Aerodynamic Dispersal Technique," Arnold Engineering Development Center Report No. AEDC-TR-71-33, March 1971.

7. Shadow, T.O., "Transonic Static Stability Characteristics of Bomblet Munition Models Used in the Evaluation of the Zero-Coning Aerodynamic Dispersal Technique," Arnold Egnineering Development Center Report No. AEDC-TR-71-247. Air Force Armament Laborabory Report No. AFATL-TR-71-144, November 1971.

8. Fletcher, C.A.J., "Wind Tunnel Tests on an Axisymmetric, Lifting Bomblet with Body Mounted, Rectangular Fins," Australian Defence Scientific Service, Weapons Research Establishment, Technical Note HSA-141, December 1968, AD 855 048.

9. Brunk, James E., Alpha Research, Inc., "Aerodynamic Dispersion Techniques," Air Force Armament Laboratory Report No. AFATL-TR-70-123, November 1970.

10. Brunk, James E. Alpha Research, Inc., "User's Manual: Extended Capability Magnus Rotor and Ballistic Body 6-DOF Trajectory Program," Air Force Armament Laboratory Report No. AFATL-TR-70-40, May 1970.

(The reverse of this page is blank)